Journal of Power Sources 241 (2013) 690–695

Contents lists available at SciVerse ScienceDirect

Journal of Power Sources

journal homepage: www.elsevier.com/locate/jpowsour

Effects of vanadium substitution on the cycling performance of olivine cathode materials

Mao-Sung Chen, She-huang Wu*, Wei Kong Pang

Department of Materials Engineering, Tatung University, Taipei 104, Taiwan, ROC

HIGHLIGHTS

- Effects of V doping on electrochemical performance of $LiFePO_4$ are studied.
- Incorporation of vanadium in $LiFePO_4$ is confirmed by the results of XRD and XAS.
- Electrochemical properties are evaluated in both half-cell and full-cell.
- Cycling performance at elevated temperature is also examined.
- Positive effects of V doping on $LiFePO_4$ cathode at 25 and 60 °C are demonstrated.

ARTICLE INFO

Article history:
Received 30 October 2012
Received in revised form
1 March 2013
Accepted 9 April 2013
Available online 30 April 2013

Keywords:
Cathode material
Lithium iron phosphate
Olivine structure
Vanadium substitution

ABSTRACT

V-substituted $LiFePO_4$ ($LiFe_{1-x}V_xPO_4$, $0 \le x \le 0.10$) powders are prepared via a solution method. The compositions, crystalline structure, morphology of the prepared powders are systemically investigated with inductive couple plasma-option emission spectrometry (ICP-OES), synchrotron radiation X-ray diffraction (s-XRD), X-ray Absorption Spectroscopy (XAS) and field emission-transmission electron microscopy (FE-TEM). Results of s-XRD and Rietveld analysis reveal that olivine phase is observed exclusively for $LiFe_{1-x}V_xPO_4$ ($x \le 0.05$) samples, whereas a minor amount of monoclinic $Li_3V_2(PO_4)_3$ is detected in the prepared $LiFe_{0.93}V_{0.07}PO_4$ and $LiFe_{0.90}V_{0.10}PO_4$ samples. It is also found that the lattice parameters of olivine structure and average Li–O and M–O (M = Fe or V) bond lengths slightly increase and decrease with the amount of V substitution, recommending an enhanced lithium diffusivity in the structure. Results of XAS study suggest that V ions occupy octahedral sites (4*c*) of Fe in $LiFePO_4$ structure with valence of 3+, showing good agreement with shortened M–O bonds determined in Rietveld analysis. As a result of V substitution, $LiFe_{1-x}V_xPO_4$, ($0 \le x \le 0.10$) cathodes exhibit better electrochemical performance, such as discharge capacity, rate capability, and cycling performance at both room and elevated temperatures.

1. Introduction

Olivine $LiFePO_4$ has been suggested as one of the most promising cathode materials for large-format lithium ion batteries for power applications since the introduction by Padhi et al. in 1997 [1,2]. $LiFePO_4$ exhibits many merits superior than other commercial cathode materials, such as potentially low cost, non-toxicity, high theoretical capacity (170 mAh g^{-1}) at 3.4 V vs. Li^+/Li, and better cycling performance [3]. However, this material suffers from its low electronic conductivity and low Li^+ ion diffusivity, hence the poor rate capability [4–6]. There are several ways have been reported to improve the rate capability of $LiFePO_4$ materials, such as coating with conductive carbon [7–14], reducing the particle size [15–17], and substitution with various cations [18–26]. Besides, its high capacity fading at elevated temperatures, which is attributed to iron dissolution into the electrolyte at temperatures higher than 45 °C, is another critical issue for commercial applications [27].

It had been demonstrated that cation substitution at Fe-sites is one of the effective approaches to overcome the abovementioned issues, i.e., poor rate capability and high capacity fading at high temperature, through the increase in mobility and diffusion coefficient of Li^+ ions as a result of lattice expansion and Li–O interaction weakening [28]. Amongst, vanadium has been suggested as an effective substitution element for this purpose. Wen et al. demonstrated that the cathode properties of olivine-structured $LiFe_{0.9}V_{0.1}PO_4$ prepared by a solid–state reaction method,

* Corresponding author. Tel.: +886 2 25922458; fax: +886 2 25936897.
E-mail address: shwu@ttu.edu.tw (S.-h. Wu).

0378-7753/$ – see front matter © 2013 Elsevier B.V. All rights reserved.
http://dx.doi.org/10.1016/j.jpowsour.2013.04.022

Table 1
Compositions of the $LiFe_{1-x}V_xPO_4$ ($0 \le x \le 0.10$) powders prepared at 700 °C. Note that P is referenced to 1 for comparison purpose.

Sample	Atomic ratio			
	Li	Fe	P	V
$LiFePO_4$	1.01(±0.1%)	0.99(±0.3%)	1	–
$LiFe_{0.99}V_{0.01}PO_4$	1.01(±0.2%)	0.99(±0.2%)	1	0.01(±0.2%)
$LiFe_{0.97}V_{0.03}PO_4$	1.00(±0.1%)	0.97(±0.2%)	1	0.03(±0.3%)
$LiFe_{0.95}V_{0.05}PO_4$	1.00(±0.1%)	0.95(±0.2%)	1	0.05(±0.1%)
$LiFe_{0.93}V_{0.07}PO_4$	1.02(±0.2%)	0.93(±0.2%)	1	0.07(±0.2%)
$LiFe_{0.90}V_{0.10}PO_4$	1.03(±0.3%)	0.90(±0.1%)	1	0.10(±0.2%)

including reversible capacity and rate capability, are better than those of pristine $LiFePO_4$ and suggested that V occupy Fe sites of the olivine structure [21]. Zhang et al. also reported similar results that $LiFe_{1-x}V_xPO_4$/C, especially at $x = 0.05$, from solid–state reaction method exhibit enhanced reversible capacity and rate capability and showed the valence of V in $LiFe_{0.95}V_{0.05}PO_4$ is between 3+ and 4+ from XAS study [29]. In contrast, Ma et al. studied $LiFePO_4$ and its derivatives prepared at 650 °C for 15 h under Ar atmosphere via a sol–gel method and claimed that the oxidation state of substituted V ions in $LiFe_{1-x}V_xPO_4$ host lattice is 4+ from XPS spectra since the binding energy positions of V-2p matched with those of represented in VO_2 [24]. Sun et al. suggested that the significantly improved high-rate charge/discharge capacity by V substitution is attributed to the increased Li^+ ion effective diffusion capability in $LiFePO_4$ lattice [23], where the transportation of Li^+ ions along the *b*-axis may be facilitated by the expansion of lattice parameters in *a* and *c* axes. In short, V substitution can significantly improve the electrochemical performance of $LiFePO_4$ cathode material for lithium ion battery. However, the valence of substituted V ions in $LiFePO_4$ and the substitution mechanism of V at atomic level remains controversial.

In this study, V-substituted $LiFePO_4$ ($LiFe_{1-x}V_xPO_4$, $0 \le x \le 0.10$) samples were prepared via a simple solution method as described elsewhere [30]. The crystalline structure, valence of V in the $LiFePO_4$ host lattice, the electrochemical properties of the prepared samples was re-studied by XRD, TEM, XAS, and capacity retention study for $LiFePO_4$//Li coin-type cells and $LiFePO_4$//MCMB pouch-type cells. Furthermore, the effects of V substitution for Fe sites on the electrochemical properties of olivine $LiFePO_4$ are discussed.

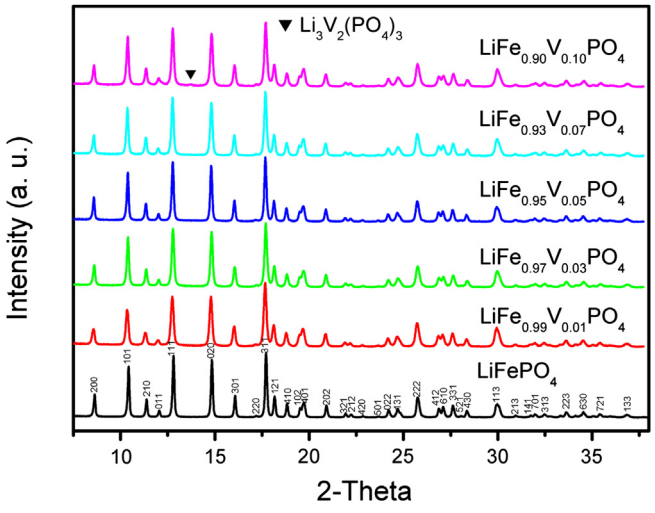

Fig. 1. Synchrotron patterns of the $LiFe_{1-x}V_xPO_4$ samples ($0 \le x \le 0.10$).

2. Experimental

V-substituted $LiFePO_4$ ($LiFe_{1-x}V_xPO_4$, $0 \le x \le 0.10$) powders were synthesized via a solution route with iron powder (NC100.24, 99%, Hoganas, Sweden), H_3PO_4 (85.0%, Wako Pure Chem. Ind., Ltd., Japan), V_2O_5 (99.0%, Wako Pure Chem. Ind., Ltd., Japan), and $LiOH \cdot H_2O$ (98.0%, Wako Pure Chem. Ind., Ltd., Japan) as starting materials. The detail of procedure is described elsewhere [30]. The starting materials were added stoichiometrically into an aqueous solution of citric acid (99.5%, Wako Pure Chem. Ind., Ltd., Japan). After iron was totally dissolved, $LiFe_{1-x}V_xPO_4$ was synthesized by a spray drying process followed by heat-treatment at 700 °C for 8 h under flowing N_2 atmosphere.

High-resolution synchrotron diffraction patterns of the prepared powders were collected at the BL01C end-station of National Synchrotron Radiation Research Center (NSRRC) of Taiwan using a constant wavelength of 0.774908 Å. Taking *Pnma* space group as the simulation model for $LiFe_{1-x}V_xPO_4$, the lattice parameters of the samples were determined by Rietveld refinement using the GSAS (General Structure Analysis System) with EXPGUI [31,32]. The compositions of Li, Fe, V, and P in the V-substituted samples were also determined by ICP-OES (Optima 2100, Perkin Elmer). The

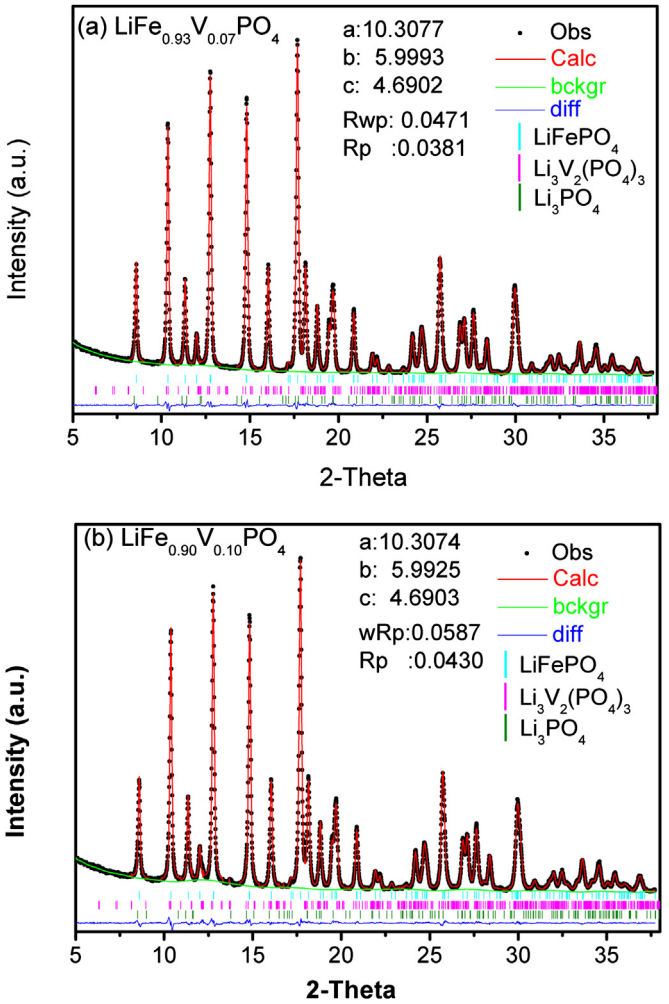

Fig. 2. Fitness profiles of GSAS refinements for synchrotron patterns of (a) $LiFe_{0.93}V_{0.07}PO_4$ and (b) $LiFe_{0.90}V_{0.10}PO_4$ samples. The vertical blue and pink lines at bottom of the figure are the standard pattern of $LiFePO_4$ and $Li_3V_2(PO_4)_3$, respectively. (For interpretation of the references to color in this figure legend, the reader is referred to the web version of this article.)

Table 2
Lattice parameters of the $LiFe_{1-x}V_xPO_4$ powders synthesized at 700 °C from Rietveld refinements. The assumption that V^{3+} ions occupy Fe^{2+} sites was made in these refinements.

Results of structural analysis obtained from Rietveld refinement of $LiFe_{1-x}V_xPO_4$, $0 \le x \le 0.10$						
Sample	$x = 0$	$x = 0.01$	$x = 0.03$	$x = 0.05$	$x = 0.07$	$x = 0.10$
Lattice constant (Å)	$a = 10.3033(1)$	$a = 10.3049(2)$	$a = 10.3060(1)$	$a = 10.3172(1)$	$a = 10.3077(1)$	$a = 10.3074(2)$
	$b = 5.9923(1)$	$b = 5.9954(1)$	$b = 5.9963(1)$	$b = 6.0015(1)$	$b = 5.9993(1)$	$b = 5.9925(1)$
	$c = 4.6856(1)$	$c = 4.6868(1)$	$c = 4.6902(1)$	$c = 4.6905(1)$	$c = 4.6902(1)$	$c = 4.6903(1)$
Lattice volume (Å^3)	289.29	289.56	289.84	290.43	290.04	289.71
Inter-atomic distances (Å)	Li–O_1:2.1278	Li–O_1:2.1297	Li–O_1:2.1428	Li–O_1:2.1564	Li–O_1:2.1420	Li–O_1:2.1445
	Li–O_2:2.0507	Li–O_2:2.0511	Li–O_2:2.0821	Li–O_2:2.0846	Li–O_2:2.0833	Li–O_2:2.0773
	Li–O_3:2.1612	Li–O_3:2.1601	Li–O_3:2.1722	Li–O_3:2.1741	Li–O_3:2.1725	Li–O_3:2.1715
	ΣLi–O:2.11(6)*	ΣLi–O:2.11(6)*	ΣLi–O:2.13(5)*	ΣLi–O:2.14(5)*	ΣLi–O:2.13(5)*	ΣLi–O:2.13(5)*
Inter-atomic distances (Å)	Fe–O_1:2.2385	Fe–O_1:2.2295	Fe–O_1:2.2244	Fe–O_1:2.1771	Fe–O_1:2.2266	Fe–O_1:2.2236
	Fe–O_2:2.1438	Fe–O_2:2.1207	Fe–O_2:2.1137	Fe–O_2:2.1079	Fe–O_2:2.1107	Fe–O_2:2.1187
	Fe–O_3:2.1688	Fe–O_3:2.1593	Fe–O_3:2.1576	Fe–O_3:2.1511	Fe–O_3:2.1566	Fe–O_3:2.1589
	ΣFe–O:2.18(5)	ΣFe–O:2.17(5)	ΣFe–O:2.17(6)	ΣFe–O:2.15(4)	ΣFe–O:2.16(6)	ΣFe–O:2.17(5)
R_{wp}	0.0572	0.0520	0.0427	0.0514	0.0471	0.0587
R_p	0.0429	0.0423	0.0338	0.0407	0.0381	0.0430
χ^2	2.306	2.322	1.947	2.226	2.202	2.485

* ΣLi–O and ΣFe–O denote as the average Li–O and Fe–O interatomic distance of the distorted octahedron.

morphologies of the samples were obtained by FEG-TEM (JEM-2100, JEOL). The XAS of the Fe and V in $LiFe_{0.95}V_{0.05}PO_4$ data were collected at BL16A of NSRRC of Taiwan. XAS data were used to determine the valences (XANES) and to study local environments (EXAFS) of substituted V in the $LiFePO_4$ host structure. The data were calibrated and analyzed using IFEFFIT (Interactive XAFS Analysis) software [33]. Firstly, energy calibration was carefully carried out by selecting a maximum point in derivative spectrum. Parameters, such as auto background removal (Rbkg = 1) and *k*-weight of 3, were applied to remove the background and to normalize the spectra ranging from 20 eV below and 30 eV above the edge, allowing directly comparison of the absorption spectra of samples with different substitution levels.

The prepared powders were mixed with a polyvinylidene fluoride (PVDF, Kynar 740, ELF, Germany) and acetylene black (99.99%, Strem Chemicals Inc., USA) in a weight ratio of 83:7:10 in N-methyl-2-pyrrolidone (NMP, ultra, ISP Technologies Inc., USA) to become slurries, respectively. Then the slurries were coated on Al foil by a doctor blade coater. After drying at 110 °C for 24 h, the tapes were punched into discs with a diameter of 10 mm for coin-type cells, and 30 × 50 mm^2 rectangular plates for pouch-type cell.

The prepared disk electrodes with a diameter of 10 mm were assembled into CR2032 coin-type cells with Li anode, Celgard 2500 separator, and 1 M $LiPF_6$ in EC: DEC (1: 1 vol. %) electrolyte (Novolyte technologies Co. Ltd, China) in an argon-filled glove box. The coin-type cells were connected to a battery tester and cycled at various current densities between 2.5 and 4.3 V for capacity retention study. The specific current used for testing is calculated based on the loading of the cathode active material. The capacity densities and active material loading (13–15 mg cm^{-2}) of the prepared cathodes were used to estimate the loading of MCMB anode for full cells preparation with the anode to cathode loading ratio of 1.05. The anode was prepared by coating slurries of MCMB, acetylene black, and PVDF binder with weight ratio of 88:6:6 in NMP solvent onto a copper foil. After drying in a vacuum oven at 110 °C for 24 h, the tape was punched into 30 × 50 mm^2 rectangular plates. $LiFePO_4$//MCMB and $LiFe_{0.95}V_{0.05}PO_4$//MCMB pouch-type cells were assembled with the rectangular anode and cathodes in an argon-filled glove box with separator and 1 M $LiPF_6$ in EC: DEC (1:1 vol. %) electrolyte. The cells were firstly activated at 10 mA g^{-1} rate between 2.5 and 3.9 V followed by cycling with 50 mA g^{-1} rate at room temperature and 60 °C. The specific current is calculated by basing it on the loading of cathode active material.

Table 3
Weight fractions of orthorhombic and monoclinic phases in prepared $LiFe_{0.93}V_{0.07}PO_4$ and $LiFe_{0.90}V_{0.10}PO_4$ samples estimated by the Rietveld method.

Sample	Wt. Fraction%	
	$LiFePO_4$	$Li_3V_2(PO_4)_3$
$LiFe_{0.93}V_{0.07}PO_4$	96.64(3)	3.36(1)
$LiFe_{0.90}V_{0.10}PO_4$	95.94(3)	4.06(3)

3. Results and discussion

From the results of ICP-OES analysis, it is found that the molar ratios among Li, Fe, V, and P of the $LiFe_{1-x}V_xPO_4$ powders synthesized at 700 °C are close to those of expected values, as shown in Table 1. From the high resolution synchrotron radiation X-ray diffraction patterns shown in Fig. 1, orthorhombic phase is observed exclusively in $LiFe_{1-x}V_xPO_4$ ($0 \le x \le 0.10$) samples prepared at 700 °C under N_2 atmosphere with $x \le 0.05$, whereas a second phase of $Li_3V_2(PO_4)_3$ is found in powers prepared with $x \ge 0.07$. The patterns were analyzed by Rietveld method using GSAS with

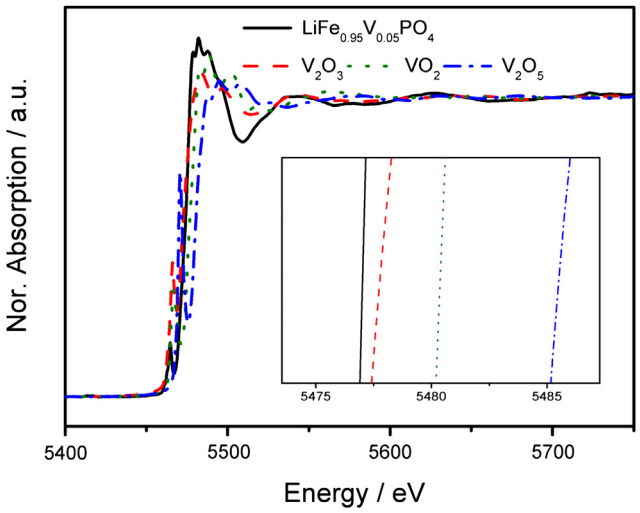

Fig. 3. Normalized absorption of V K-edge for $LiFe_{0.95}V_{0.05}PO_4$ sample along with the references of V_2O_3, VO_2, and V_2O_5.

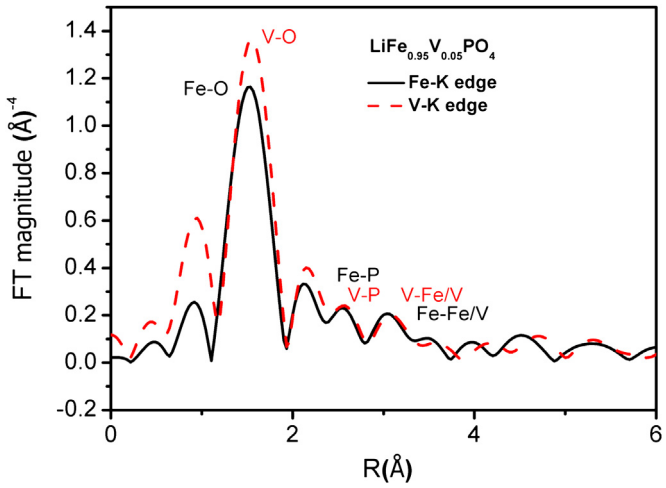

Fig. 4. Results of k^2-weighted FT EXAFS spectra with Fe K-edge and V K-edge for $LiFe_{0.95}V_{0.05}PO_4$.

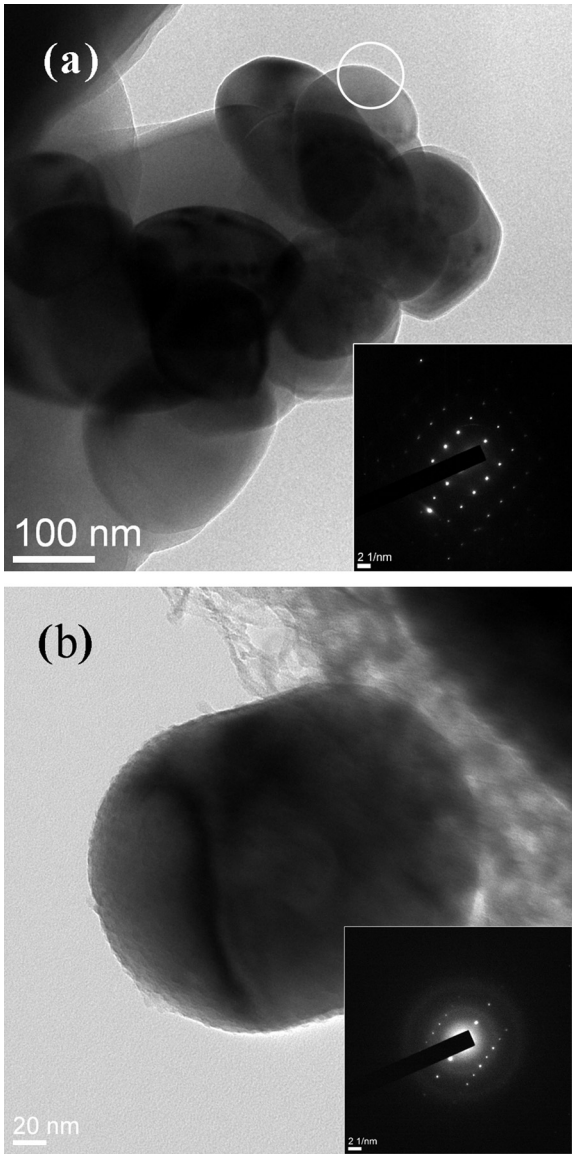

Fig. 5. TEM photographs of the prepared (a) $LiFePO_4$ and (b) $LiFe_{0.95}V_{0.05}PO_4$ powders. Inset shows the electron diffraction of the selected area.

EXPGUI program. The fitness profiles of refinement works are shown in Fig. 2a and b and the refinement results are listed in Tables 2 and 3. It can be found that the lattice parameters of orthorhombic phase in the prepared samples increase with amount of V substitution up to $x = 0.05$. Moreover, Li—O interatomic distances are also lengthened by V-substitution and exhibit a maximum value at $x = 0.05$. The regular shifts of the lattice parameters imply that the alien elements V has been successfully occupied 4*c* sites of Fe^{2+} in the $LiFePO_4$ structure to form solid solution $LiFe_{1-x}V_xPO_4$. Table 3 shows the calculated weight fractions of orthorhombic $LiFePO_4$ and monoclinic $Li_3V_2(PO_4)_3$ phases in the prepared $LiFe_{0.93}V_{0.07}PO_4$ and $LiFe_{0.90}V_{0.10}PO_4$. The existence of second phase $Li_3V_2(PO_4)_3$ at $x \geq 0.07$ indicates that the saturation of V substitution for Fe may be achieved when $0.05 \leq x \leq 0.07$. As $Li_3V_2(PO_4)_3$ is formed, the substitution level of V in $LiFe_{1-x}V_xPO_4$ would be lower than the anticipated *x* value. For example, at $x = 0.07$, the amount of $Li_3V_2(PO_4)_3$ is determined to be around 3.4 wt.%, suggesting the actual substitution level of V is lower than 0.05. From the calculated lattice parameter and Li—O results, the substitution level of V is close to 0.03, indicating the preferential formation of $Li_3V_2(PO_4)_3$ than $LiFe_{1-x}V_xPO_4$ at excess V amount.

In order to confirm the oxidation state and the site occupation of vanadium ions in the prepared samples, X-ray absorption near edge structure (XANES) and extended X-ray absorption fine structure (EXAFS) measurements were also carried out. By comparing the spectrum of $LiFe_{0.95}V_{0.05}PO_4$ at V K-edge to those of V^{3+}-, V^{4+}-, and V^{5+}-reference compounds (V_2O_3, VO_2, and V_2O_5, respectively) shown in Fig. 3, it reveals that vanadium absorption edge of the prepared $LiFe_{0.95}V_{0.05}PO_4$ appears V_2O_3. This observation recommends that the valence of V in the V-substituted orthorhombic sample is 3+ [23]. As shown, the pre-edge peak decreases in intensity with V. Given that a distorted octahedron VO_6 contributes an intense pre-edge peak in XANES spectra [34], the less intensity pre-edge can be possibly ascribed to the distortion of VO_6 octahedra turning into a regular geometry in olivine structure, further suggesting the substituted V reside at octahedral site of the host structure. The magnitudes of Fourier transforms (FTs) of k^2 weighted EXAFS spectra (radical structure function) were calculated and plotted in Fig. 4. Both the curves manifest three main well-defined peaks, due to the M—O, M—P, and M—M (M = Fe or V) interactions in the olivine structure at 1.54, 2.55, 3.04 Å, respectively. The FT features of substituted V are almost identical to that of Fe in the olivine $LiFePO_4$, indicating the scattering contribution of

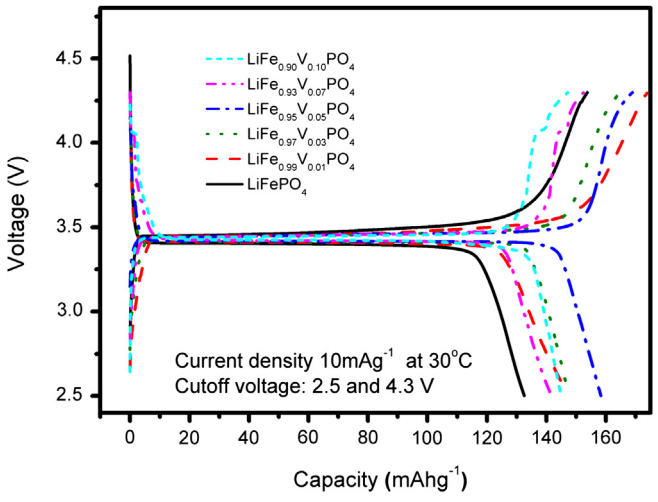

Fig. 6. Initial charge/discharge curves of the coin-type cells comprised with prepared $LiFe_{1-x}V_xPO_4$ ($0 \leq x \leq 0.10$) cathodes at current density 10 mA g^{-1}.

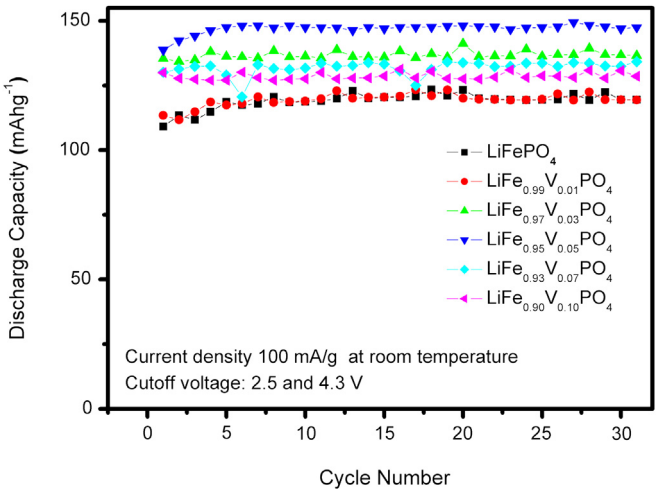

Fig. 7. Results of capacity retention study of the coin-type cells comprised with $LiFe_{1-x}V_xPO_4$ ($0 \le x \le 0.10$) cathodes cycled at 100 mA g^{-1} at room temperature.

different atomic shells around the X-ray adsorbing vanadium and iron ions and suggesting V ions occupy Fe sites in the host structure. Reconciling with XANES results, it can be concluded that substituted V ions occupy octahedral sites of Fe and exhibit a trivalent oxidation state in the olivine structure.

Fig. 5a and b show the morphology and the selected-area electron diffraction (SAD) patterns of the prepared $LiFePO_4$ and $LiFe_{0.95}V_{0.05}PO_4$ particles, respectively. The spot diffraction patterns obtained indicate that $LiFePO_4$ and $LiFe_{0.95}V_{0.05}PO_4$ are both well crystallized. As calculated from the SAD patterns, d_{311} of olivine $LiFe_{0.95}V_{0.05}PO_4$ was obtained to be around 2.547 Å, which is slightly larger than that of the un-substituted $LiFePO_4$ (2.525 Å). This result shows great agreement with the synchrotron radiation diffraction results.

The initial galvanostatic charge and discharge curves of the $LiFe_{1-x}V_xPO_4$ coin-type cells cycled with a constant current density of 10 mA g^{-1} between cutoff voltages of 2.5 and 4.3 V at room temperature are shown in Fig. 6. The initial discharge capacities of 132, 147, 147, 158, 141, and 144 mAh g^{-1} were obtained from cells comprised with $LiFe_{1-x}V_xPO_4$ samples ($x = 0$, 0.01, 0.03, 0.05, 0.07, and 0.10), respectively. Among the prepared samples,

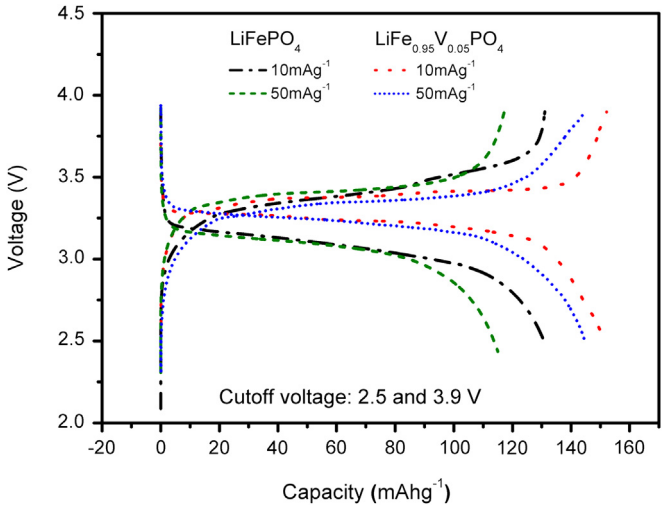

Fig. 9. The charge/discharge curves of the formation cycle with 10 mA g^{-1} and initial cycle at 50 mA g^{-1} of $LiFePO_4$//MCMB pouch-type cell comprised with prepared $LiFePO_4$ and $LiFe_{0.95}V_{0.05}PO_4$//MCMB cathodes. (The applied current density is based on the loading of cathode active material).

$LiFe_{0.95}V_{0.05}PO_4$ exhibits the highest capacity in the initial cycle. It agrees with the results reported by Zhang et al. [29]. Potential plateaus at 4.06/4.08 V are also observed on the charge/discharge curves of the samples prepared with $x \ge 0.07$, which is due to the existence of $Li_3V_2(PO_4)_3$ phase. The results are inconsistent with those obtained from XRD study. Fig. 7 shows the results of capacity retention study of the coin-type cells comprised with $LiFe_{1-x}V_xPO_4$ ($0 \le x \le 1.0$) samples at 100 mA g^{-1} rate at room temperature. As shown, $LiFe_{0.95}V_{0.05}PO_4$ sample exhibits the highest reversible capacity of 148 mAh g^{-1} among the prepared $LiFe_{1-x}V_xPO_4$ ($0 \le x \le 0.10$) powders. By comparing with the results of the cells cycled at a current density of 1000 mA g^{-1}, shown in Fig. 8, the $LiFe_{0.95}V_{0.05}PO_4$ sample also shows improved rate capability. That may be due to the increased Li^+ ion diffusivity by the larger lattice parameters and longer Li–O interatomic distances induced by V substitution, shown in Table 2, than those of pristine $LiFePO_4$ [28].

The charge/discharge curves of the formation cycle at a current density of 10 mA g^{-1} and the initial cycle at 50 mA g^{-1} of the

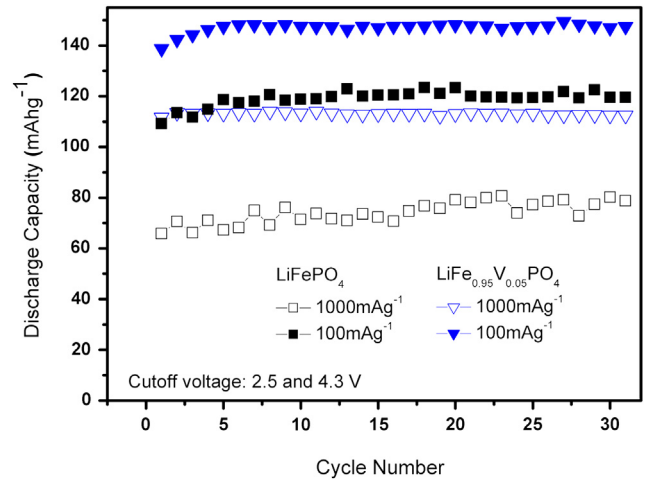

Fig. 8. Results of capacity retention study of the coin-type cells comprised with $LiFePO_4$ and $LiFe_{0.95}V_{0.05}PO_4$ cathodes cycled at 100 and 1000 mA g^{-1} at room temperature.

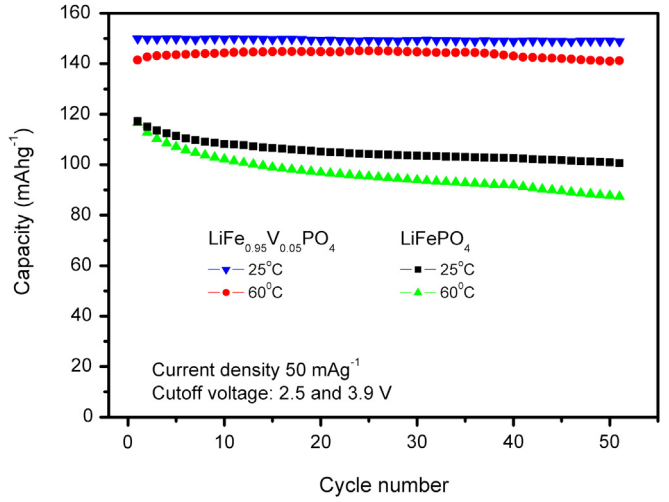

Fig. 10. Cycling performance of the $LiFePO_4$//MCMB and $LiFe_{0.95}V_{0.05}PO_4$//MCMB cells with 50 mA g^{-1} after formation at 25 and 60 °C.

prepared $LiFe_{1-x}V_xPO_4$//MCMB pouch-type cells comprised with synthesized $LiFePO_4$ cathodes are shown in Fig. 9. The cell prepared with $LiFe_{0.95}V_{0.05}PO_4$ shows smaller polarization (voltage difference between charge/discharge plateaus) than that of the cell prepared with pristine sample. The $LiFe_{0.95}V_{0.05}PO_4$//MCMB cell exhibits higher initial discharge capacity of 145 mAh g^{-1} after formation but also shows lower capacity fading rate than those of pouch-type cell comprised with $LiFePO_4$ when cycling at 50 mA g^{-1} up to 30 cycles, as shown in Fig. 10. It can also be found that the capacity fading rate increases from 0.34 at 25 °C to 0.57 mAh g^{-1} $cycle^{-1}$ when $LiFePO_4$/MCMB cell is cycled at 60 °C with the same rate, while the fading rate of the $LiFe_{0.95}V_{0.05}PO_4$//MCMB cell increases from 0.02 at 25 °C to 0.14 mAh g^{-1} $cycle^{-1}$ at 60 °C. It may be due to the enhanced Li^+ ion diffusivity and structure stability in $LiFe_{0.95}V_{0.05}PO_4$ structure.

4. Conclusions

$LiFe_{1-x}V_xPO_4$ ($0 \leq x \leq 0.10$) powders were synthesized via a solution route followed by heat-treatment at 700 °C under flowing N_2 atmosphere. Olivine phase was found exclusively in samples prepared with $x \leq 0.05$, whereas $Li_3V_2(PO_4)_3$ phase was also found in the samples prepared with $x \geq 0.07$. Synchrotron radiation diffraction and Rietveld analysis revealed that the lattice parameters of the olivine structure increase with amount of V substitution. XANES and EXAFS results suggested that vanadium exhibits a valence of 3+ and resides at Fe sites (4*c*) in olivine structure. $LiFe_{0.95}V_{0.05}PO_4$ sample shows the best electrochemical performance, such as reversible capacity, rate capability, and capacity retention rate at elevated temperature.

Acknowledgments

The study had been financially supported by the National Science Council (NSC) of Taiwan and Tatung University. The authors are also grateful for the instrumental supports by NSRRC and Academia Sinica of Taiwan.

References

[1] A.K. Padhi, K.S. Nanjundaswamy, J.B. Goodenough, J. Electrochem. Soc. 144 (1997) 1188–1194.
[2] A.K. Padhi, K.S. Nanjundaswamy, C. Masquelier, S. Okada, J.B. Goodenough, J. Electrochem. Soc. 144 (1997) 1609–1613.
[3] A.S. Andersson, B. Kalska, L. Häggström, J.O. Thomas, Solid State Ionics 130 (2000) 41–52.
[4] P.P. Prosini, M. Lisi, D. Zane, M. Pasquali, Solid State Ionics 148 (2002) 45–51.
[5] A. Yamada, S.C. Chung, K. Hinokuma, J. Electrochem. Soc. 148 (2001) A224–A229.
[6] S.-Y. Chung, J.T. Bloking, Y.-M. Chiang, Nat. Mater. 1 (2002) 123–128.
[7] R. Dominko, M. Bele, M. Gaberscek, M. Remskar, D. Hanzel, S. Pejovnik, J. Jamnik, J. Electrochem. Soc. 152 (2005) A607–A610.
[8] M.-R. Yang, T.-H. Teng, S.-H. Wu, J. Power Sources 159 (2006) 307–311.
[9] Y. Zhou, C.D. Gu, J.P. Zhou, L.J. Cheng, W.L. Liu, Y.Q. Qiao, X.L. Wang, J.P. Tu, Electrochim. Acta 56 (2011) 5054–5059.
[10] D. Lepage, C. Michot, G. Liang, M. Gauthier, S.B. Schougaard, Angew. Chem. Int. Ed. 50 (2011) 6884–6887.
[11] B. Pei, Q. Wang, W. Zhang, Z. Yang, M. Chen, Electrochim. Acta 56 (2011) 5667–5672.
[12] H. Huang, S.-C. Yin, L.F. Nazar, Electrochem. Solid-State Lett. 4 (2001) A170–A172.
[13] Z. Chen, J.R. Dahn, J. Electrochem. Soc. 149 (2002) A1184–A1189.
[14] C.H. Mi, Y.X. Cao, X.G. Zhang, X.B. Zhao, H.L. Li, Powder Technol. 181 (2008) 301–306.
[15] C.M. Julien, A. Mauger, K. Zaghib, J. Mater. Chem. 21 (2011) 9955–9968.
[16] D.-H. Kim, J. Kim, J. Phys, Chem. Solids 68 (2007) 734–737.
[17] D.-H. Kim, J. Kim, Electrochem. Solid-State Lett. 9 (2006) A439–A442.
[18] H. Liu, C. Li, Q. Cao, Y. Wu, R. Holze, J. Solid State Electrochem. 12 (2008) 1017–1020.
[19] G. Wang, Y. Cheng, M. Yan, Z. Jiang, J. Solid State Electrochem. 11 (2007) 457–462.
[20] H. Liu, Q. Cao, L.J. Fu, C. Li, Y.P. Wu, H.Q. Wu, Electrochem. Commun. 8 (2006) 1553–1557.
[21] Y. Wen, L. Zeng, Z. Tong, L. Nong, W. Wei, J. Alloys Compd. 416 (2006) 206–208.
[22] M.-R. Yang, W.-H. Ke, J. Electrochem. Soc. 155 (2008) A729–A732.
[23] C.S. Sun, Z. Zhou, Z.G. Xu, D.G. Wang, J.P. Wei, X.K. Bian, J. Yan, J. Power Sources 193 (2009) 841–845.
[24] J. Ma, B. Li, H. Du, C. Xu, F. Kang, J. Electrochem. Soc. 158 (2011) A26–A32.
[25] T. Nakamura, Y. Miwa, M. Tabuchi, Y. Yamada, J. Electrochem. Soc. 153 (2006) A1108–A1114.
[26] J. Barker, M.Y. Saidi, J.L. Swoyer, Electrochem. Solid-State Lett. 6 (2003) A53–A55.
[27] K. Amine, J. Liu, I. Belharouak, Electrochem. Commun. 7 (2005) 669–673.
[28] D. Wang, H. Li, S. Shi, X. Huang, L. Chen, Electrochim. Acta 50 (2005) 2955–2958.
[29] L.-L. Zhang, G. Liang, A. Ignatov, M.C. Croft, X.-Q. Xiong, I.M. Hung, Y.-H. Huang, X.-L. Hu, W.-X. Zhang, Y.-L. Peng, J. Phys. Chem. C 115 (2011) 13520–13527.
[30] S.-H. Wu, K.-M. Hsiao, W.-R. Liu, J. Power Sources 146 (2005) 550–554.
[31] A.C. Larson, R.B.V. Dreele, Los Alamos National Laboratory Report LAUR, 1994, pp. 86–748.
[32] B.H. Toby, J. Appl. Crystallogr. 34 (2001) 210–213.
[33] B. Ravel, M. Newville, Phys. Scr. 2005 (2005) 1007.
[34] J. Wong, F.W. Lytle, R.P. Messmer, D.H. Maylotte, Phys. Rev. B 30 (1984) 5596–5610.